Published by Nigerian Society of Physical Sciences. Hosted by FLAYOO Publishing House LTD

Recent Advances in Natural Sciences

Journal Homepage: https://flayoophl.com/journals/index.php/rans

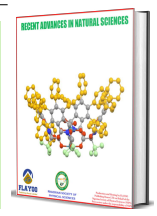

Synthesis and characterization of biodiesel from black date (*Canarium schweinfurtii*) seed kernel oil in the presence of green-synthesized Cu-Mn/TiO_2 nanocatalyst using central composite design approach

J. Mohammed [a,*], M. O. Aremu[b], A. Usman[b]

[a]*Department of Chemistry, Faculty of Natural & Applied Sciences, Nasarawa State University, Keffi, Nigeria*
[b]*Department of Chemistry, Faculty of Physical Sciences, Federal University Lafia, Nigeria*

ARTICLE INFO

Article history:
Received: 14 August 2025
Received in revised form: 01 January 2026
Accepted: 02 January 2026
Available online: 06 April 2026

Keywords: Transesterification, Black date, Biodiesel, Nano catalyst, Central composite design

DOI:10.61298/rans.2026.4.1.227

ABSTRACT

One of the key challenges in scaling up biodiesel production is attaining the maximum yield while ensuring compliance with established quality standards. In this work, the potential of black date seed kernel oil as a feedstock for biodiesel synthesis was investigated using a green-synthesized Cu-Mn/TiO_2 nanocatalyst through a transesterification process. The oil was characterized using standard analytical procedures, while the catalyst was analyzed through FTIR, XRD, BET, and SEM techniques. Process optimization was carried out using Central Composite Design (CCD), considering methanol-to-oil molar ratio, catalyst loading, reaction temperature, and reaction time as the key variables. The optimum biodiesel yield of 95.07% was achieved at a methanol-to-oil molar ratio of 12:1, catalyst loading of 2 wt%, reaction temperature of 65 ˚C, and reaction time of 75 minutes. The quadratic model developed from the experimental design was statistically significant ($p < 0.0001$), confirming its predictive reliability. The high coefficient of determination ($R^2 = 0.9904$), along with adjusted R^2 (0.9815) and predicted R^2 (0.9449) values obtained from ANOVA and fit statistics, demonstrated a strong agreement between the experimental and predicted outcomes. Among the studied variables, all exhibited significant effects on biodiesel yield except the methanol-to-oil molar ratio ($p > 0.05$). Physicochemical analysis of the oil confirmed its suitability as a feedstock for biodiesel production. These findings highlight black date seed kernel oil as a promising non-edible and sustainable raw material for biodiesel synthesis, contributing to the advancement of renewable and eco-friendly fuel alternatives.

1. INTRODUCTION

The continued reliance on fossil fuels as a primary energy source has long been recognized as unsustainable due to their finite reserves and their significant role in elevating atmospheric carbon dioxide levels through combustion, thereby intensifying greenhouse gas emissions and global warming [1, 2]. Data from

*Corresponding author Tel. No.: +234-706-8747-388
e-mail: jibrinmohammed@nsuk.edu.ng (J. Mohammed)

the Bureau of Statistical Review of World Energy (2021) indicate that global fossil fuel consumption reached approximately 13.541 billion metric tons in 2014, representing a 122% increase compared to 1973 levels. If this upward trend persists, crude oil reserves could be depleted by 2052 [3]. Environmentally, it is estimated that the combustion of fossil fuels in diesel engines releases about 15 billion tons of carbon dioxide (CO_2) annually, a primary driver of global warming [4, 5], with projections suggesting an additional 1.3 billion tons of CO_2 emissions by 2030 [5].

Given these concerns, researchers have emphasized the urgent need for alternative, sustainable energy solutions. Biofuels have emerged as a promising option due to their renewability, high energy content, biodegradability, and lower environmental impact compared to petroleum-based fuels [5–7]. Reports from the E.U. International Energy Agency and the U.S. Department of Energy suggest that substituting fossil fuels with biofuels could achieve up to a 50% reduction in CO_2 emissions by 2050 [8]. Biofuel is defined as combustible fuel derived from recently produced biomass such as crops, crop residues, grasses, wood, fibers, and even industrial or municipal wastes unlike fossil fuels, which originate from ancient biomass deposits [9–11].

Biodiesel is a renewable biofuel derived from various feedstocks, including edible vegetable oils such as soybean, groundnut, palm, and sunflower oils, as well as non-edible oils like jatropha, polanga, algae, and neem oils. It is commonly produced via the transesterification process, in which oils react with alcohol in the presence of a catalyst, generating glycerol as a by-product. Due to its close physicochemical resemblance to petroleum diesel, biodiesel is widely regarded as one of the most promising sustainable alternatives capable of replacing conventional diesel fuels [12, 13].

Nonetheless, as reported by Akhabue et al. [13], a major challenge in biodiesel production lies in the heavy reliance on edible oil feedstocks, which can trigger competition between food and fuel, potentially leading to food scarcity. This competition also elevates production costs, as increasing demand drives up feedstock prices [14]. To mitigate this issue, the use of non-edible oils is strongly recommended. One example is oil from *Canarium schweinfurthii* seed kernel, a valuable non-edible resource for biodiesel synthesis. This tall, evergreen forest tree offers multiple benefits and is predominantly found in Nigeria's Northern and Eastern regions, where it is locally known as "black date" in English, "ube" in Igbo, and "atile" in Hausa [15]. Its fruit yields two types of oil, one from the pulp and another from the kernel, each containing approximately 40-50% oil [15].

The efficiency of the transesterification process depends on several parameters, including feedstock type, alcohol-to-oil molar ratio, catalyst type, reaction temperature and time, mixing intensity, moisture content, and free fatty acid levels [3, 8]. Furthermore, literature indicates that the choice of catalyst significantly affects biodiesel productivity and scalability. Conventional homogeneous catalysts (e.g., NaOH, KOH) and heterogeneous catalysts (e.g., CaO, MgO) present drawbacks such as soap formation, limited reusability, high energy demands, and complex separation steps [15–17]. Recent advances have identified nanocatalysts as a promising solution to these limitations, owing to their high surface-area-to-volume ratio, superior mass transfer properties, adjustable surface chemistry, and excellent thermal stability. These features enhance biodiesel yield, shorten reaction time, and enable catalyst recycling [16, 18]. In the present study, a green-synthesized Cu-Mn/TiO_2 nanocatalyst, prepared via the coprecipitation method using orange peel extract, was employed for biodiesel production from black date seed kernel oil.

Based on the reviewed literature, it is clear that biodiesel production is a complex process influenced by multiple factors that collectively determine its quality, cost-effectiveness, and environmental impact. Addressing these challenges requires the integration of advanced computational techniques, with Response Surface Methodology (RSM) being particularly valuable for process refinement and optimization. RSM is a powerful statistical approach used to model, analyze, and optimize processes by examining the interactions between several input variables and assessing their combined influence on a target response [18].

In this study, the Central Composite Design (CCD), a variant of RSM, was applied to systematically optimize the key process variables for biodiesel synthesis from African black date seed (kernel) oil. The research specifically aimed to enhance biodiesel yield through catalytic transesterification using a green-synthesized Cu-Mn/TiO_2 nanocatalyst, while employing CCD to determine the optimal operating conditions for maximum production efficiency.

2. MATERIALS AND METHODS

2.1. MATERIALS

2.1.1. Chemicals and reagents

Titanium(IV) nitrate ($Ti(NO_3)_4$, CAS No. 13826-86-3), manganese(II) acetate tetrahydrate ($Mn(CH_3COO)_2{\cdot}4H_2O$, CAS No. 6156-78-1), and copper(II) nitrate hydrate ($Cu(NO_3)_2{\cdot}2.5H_2O$, CAS No. 19004-19-4) were purchased from Sigma-Aldrich (Merck), Sodium thiosulphate ($Na_2S_2O_3{\cdot}5H_2O$, CAS No. 10102-17-7), potassium hydroxide (KOH, CAS No. 1310-58-3), sodium hydroxide (NaOH, CAS No. 1310-73-2), hydrochloric acid (37%, CAS No. 7647-01-0), sulphuric acid (CAS No. 7664-93-9), acetic acid (CAS No. 64-19-7), potassium iodide (CAS No. 7681-11-0), n-hexane (CAS No. 110-54-3) all from BDH Chemicals. Other chemicals and reagents used were of analytical grade and employed without any treatment.

2.1.2. Instruments

A FTIR spectrometer (Perkin Elmer, 100), X-ray diffractometer (XRD) (Shimadzu XRD-6000, Japan) operated at 30 kV and 30 mA with CuKα radiation (λ = 0.1541 nm) and 2θ ranging from 10 to 80°, BET analysis was carried out using N_2 adsorption/desorption analyzer (Thermo-Finnigan Sormatic 1990 series) and scanning electron microscopy (SEM) instrument (JOEL, JSM-6480A Japan) operated at 20 kV.

2.2. SAMPLE COLLECTION AND PREPARATION

Waste black date (*Canarium schweinfurthii*) fruits were sourced from a local fruit market in Jos South Local Government Area, Plateau State, Nigeria. The seeds were manually separated from the fruit pulp, and the shells were cracked open using a small hammer to obtain the kernels. The kernels were air-dried in the laboratory for two weeks, ground into a fine powder, and stored

in airtight plastic containers for subsequent analysis. Analytical-grade n-hexane and methanol were used for the oil extraction and transesterification processes, respectively.

2.3. OIL EXTRACTION

Oil was extracted from the powdered seed sample using the solvent extraction method. A 15 g portion of the sample was placed in a Soxhlet extractor containing 200 ml of n-hexane as the solvent. The extraction was carried out at 60 ˚C for 6 hours. After extraction, the mixture was concentrated using a rotary evaporator to recover the solvent, followed by further drying in a fume hood for 48 hours to remove residual solvent [19, 20]. This process was repeated until an adequate quantity of oil was obtained. The oil yield was calculated using:

$$\text{Oil yield } (\%) = \frac{W_2 - W_0}{W_1} \times 100, \tag{1}$$

where W_1 = weight of sample (g), W_2 = weight of flask + oil (g) and W_0 = weight of flask (g).

2.4. CHARACTERIZATION OF THE EXTRACTED OIL

The physicochemical properties of the *Canarium schweinfurthii* kernel oil, including density, specific gravity, moisture content, kinematic viscosity, saponification value, acid value, iodine value, peroxide value, and free fatty acid (FFA) content, were determined in accordance with ASTM standard procedures [3, 17, 19].

2.4.1. Determination of moisture content

The oil sample (2.0 g) was placed in an oven at 105 ˚C for 2 h, then cooled and weighed repeatedly until a constant weight was achieved. The moisture content was calculated using [3]:

$$\text{Moisture } (\%) = \frac{W_1 - W_2}{W_1 - W_0} \times 100, \tag{2}$$

where, W_0= weight of the empty crucible (g), W_1 = weight of the prepared sample + empty crucible (g) and W_2 = weight of dried sample + empty crucible (g).

2.4.2. Determination of specific gravity (SG)

The specific gravity of the sample was measured using a 50 ml measuring cylinder of known weight. The cylinder was first cleaned, dried, and recorded as W_0. Next, 5 ml of the sample was added, and the total weight was noted as W_1. The sample weight was then obtained by subtracting the empty cylinder weight (W_0) from the filled cylinder weight (W_1). The specific gravity of the oil was determined using [17]:

$$\text{SG} = \frac{W_1 - W_0}{W_2}, \tag{3}$$

where W_1 = weight of the cylinder + oil (g) W_0 = weight of cylinder (g) and W_2 = weight of equal volume of water (g).

2.4.3. Determination of density

The density of the oil was determined using the same procedure for specific gravity. The density was calculated using [19]:

$$\text{Density} = \frac{W_1 - W_0}{V}, \tag{4}$$

where W_1 = weight of the cylinder + oil (g) W_0 = weight of cylinder (g) and V = volume of the oil (cm^3).

2.4.4. Determination of free fatty acid (FFA)/Acid value

The oil sample (2.0 g) was dissolved in 30 ml of highly purified ethanol and heated in a water bath for 2 min. The resulting solution was then titrated with 0.1 M potassium hydroxide (KOH) using phenolphthalein as an indicator until a persistent pink color appeared [19]. The free fatty acid and acid value were calculated using Eqs. (5) and (6), respectively.

$$\text{FFA } (\%) = \frac{V \times C \times 282.47}{M} \times 100, \tag{5}$$

$$\text{Acid value (mgKOH/g)} = \frac{V \times C \times 56.1}{M}, \tag{6}$$

where V = volume of potassium hydroxide solution (cm^3), C = concentration of potassium hydroxide solution (mol/dm^3), M = mass of the oil sample (g), 282.47 = molar mass of oleic acid, and 56.1 = molar mass of potassium hydroxide (g/mol).

2.5. PEROXIDE VALUE (PV)

The oil sample (2.5 g) was placed into a 100 ml conical flask, and 10 ml of chloroform was added to dissolve the sample with gentle stirring. Then, 15 ml of acetic acid and 1 ml of freshly prepared saturated potassium iodide solution were introduced. The flask was immediately sealed, shaken for 1 min, and left in the dark at room temperature for 5 min. Subsequently, 75 ml of distilled water was added, and the liberated iodine was titrated with 0.01 M sodium thiosulfate solution. A blank test was also performed following the same procedure. The peroxide value was calculated using [19]:

$$\text{Peroxide value} = \frac{(V_1 - V_0) \times T \times 1000}{M}, \tag{7}$$

where V_0 = volume of the sodium thiosulphate solution used for blank, V_1 = volume of the sodium thiosulphate solution used for determination of the sample, T = the concentration of the sodium thiosulphate used, and M = mass of oil sample (g).

2.5.1. Determination of iodine value (IV)

The oil sample (2.0 g) was dissolved in 20 ml of chloroform, after which 25 ml of Hanus iodine solution (I_2 + Br/ACOH) was added. The mixture was kept in the dark for 30 min. Then, 10 ml of 15% potassium iodide solution and 100 ml of freshly distilled water were added. The liberated iodine was titrated with 0.1 M sodium thiosulphate until the yellow color nearly disappeared. A few drops of 1% starch solution were added as an indicator, and titration continued until the blue color completely disappeared. A blank test was conducted under the same conditions using 25 ml of Hanus solution and sodium thiosulphate without the sample [17]. The iodine value was calculated using:

$$\text{Iodine value} = \frac{(V_1 - V_2) \times C \times 12.69}{M}, \tag{8}$$

where C = concentration of sodium thiosulphate (mol/dm^3), V_1 = Volume of sodium thiosulphate solution used for blank test (cm^3), V_2 = volume of sodium thiosulphate solution used for determination (cm^3), and M = mass of the oil sample (g).

2.5.2. Saponification value (SV)

The oil sample (5.0 g) was refluxed with 50 ml of 0.5% alcoholic potassium hydroxide for approximately 30 min. The mixture was then allowed to cool for 10 min before being titrated with 0.5 M hydrochloric acid solution, using a drop of phenolphthalein as an indicator, until the pink coloration disappeared. A blank test was also carried out under the same conditions, using only the alcoholic potassium hydroxide solution without the oil sample. The saponification value was determined using [3]:

$$\text{Saponification value} = \frac{(V_1 - V_0) \times T \times 56.1}{M} \text{ mg KOH}, \quad (9)$$

where T = molar concentration of KOH (mol/dm^3), V_0 = volume of acid used for the titration with the oil sample (cm^3), V_1 = volume of acid used for the titration of the blank solution (cm^3), and M = mass of the oil sample (g).

2.5.3. Kinematic viscosity

The oil sample was first purified using a sintered glass filter and then introduced into a viscometer (Ostwald Type A) through suction in a viscometer bench setup. The viscometer bath was maintained at 40 ˚C, and the sample was equilibrated in the bath for 20 min. Suction was applied to raise the sample slightly above the upper timing mark, after which the efflux time was recorded as the sample flowed freely from the upper to the lower timing mark. The viscosity was determined using [17]:

$$\text{Kinetic viscosity} = T \times K, \quad (10)$$

where T = efflux time and K = viscometer constant

2.6. DETERMINATION OF CALORIFIC VALUE

The calorific value of the biodiesel was determined using a bomb calorimeter (IKA C5000), following the ASTM D240 standard. Before the test, the biodiesel sample was filtered to remove impurities and oven-dried at 105 ˚C for 1 h to eliminate residual moisture, as water can interfere with accuracy by absorbing heat during combustion. About 1.0 g of the dried sample was precisely weighed (±0.1 mg) into a clean, pre-weighed stainless-steel crucible and placed inside the bomb combustion chamber. An ignition wire was positioned in contact with the fuel, after which the chamber was sealed and charged with high-purity oxygen at 30 atm to ensure complete combustion. The bomb was then immersed in the calorimeter's water jacket containing 2000 g of distilled water, and the initial water temperature was recorded. Combustion was initiated electrically, and the resulting rise in water temperature was measured using a high-precision thermometer. The calorific value was calculated from the observed temperature rise using [17]:

$$\text{Calorific value} = \frac{(M_w C_p + W_c)\Delta T}{M}, \quad (11)$$

where M_w = mass of water in the calorimeter (kg), C_p = specific heat capacity of water (4.187 kJ/kg·˚C), ΔT = change in temperature (˚C), W_c = water equivalent (heat capacity) of the calorimeter (kJ/˚C) and M = mass of biodiesel sample (kg)

2.7. CETANE NUMBER (CN)

The method used by Ref. [3] was employed. The calculated saponification value (SV) and iodine value (IV) were used to calculate the cetane number (CN) of the biodiesel. The cetane number was determined using:

$$\text{Cetane Number (CN)} = 46.3 + \frac{5458}{\text{SV}} - 0.225 \times \text{IV}. \quad (12)$$

2.8. FLASH POINT DETERMINATION

The flash point of the biodiesel sample was measured following the method of Ref. [17]. For each sample, 10 ml was placed in a clean aluminum container and heated over a Bunsen burner at approximately 10 ˚C/min. A thermometer was inserted into the liquid, and at every 5 ˚C increment, a small test flame was passed just above the sample's surface until a distinct flash was observed. The temperature at which this flash occurred was recorded as the flash point.

2.9. POUR POINT DETERMINATION

The pour point was determined as described by Ref. [17]. About 5 ml of the oil/biodiesel was transferred into a test tube, into which a calibrated thermometer (with graduations below 1 ˚C) was inserted. The tube was then immersed in an ice bath and left until the sample solidified. Afterward, the tube was removed, tilted slightly, and carefully observed until the first signs of flow appeared. The temperature at which movement was detected was recorded as the pour point.

2.10. SULPHUR CONTENT DETERMINATION

Sulphur content was analyzed using a UV fluorescence sulphur analyzer (LECO S832) in accordance with ASTM D5453 [17]. A 20 µL aliquot of the biodiesel sample was introduced into a quartz combustion tube maintained at ~1100 ˚C under a continuous flow of ultra-high-purity oxygen (99.99%). During combustion, sulphur compounds were oxidized to sulphur dioxide (SO_2), which was carried through a moisture trap into the UV fluorescence detector. The emitted fluorescence from the excited SO_2 molecules was measured and quantified against a calibration curve prepared with certified sulphur standards in biodiesel. Calibration was performed over a low-sulphur range (0.05-50 ppm), and blank runs were included to correct for background interference.

2.11. DETERMINATION OF FATTY ACID PROFILE

The fatty acid composition of the *Canarium schweinfurthii* kernel oil was determined using Gas Chromatography-Mass Spectrometer (GC-MS) (SHIMADZU TQ8040, Maryland, USA). The oil sample was dissolved in a n-hexane-to-acetone solvent mixture (4:1 v/v). High-purity helium gas (99.999%) was used as the carrier at a flow rate of 1 mL/min with a split ratio of 4:1 (v/v). A 100 µL aliquot of the prepared sample was injected into the GC column at an inlet temperature of 250 ˚C. The injector and detector temperatures were maintained at 280 ˚C. The column temperature program began at 60 ˚C (held for 5 min), then increased by 5 ˚C/min to a final temperature of 280 ˚C with no hold time. The ion source temperature was set to 200 ˚C. Fatty acids were identified by comparing the obtained mass spectra with reference

library data, considering relative abundance, molecular formula, molecular weight, and structural information [21].

2.12. PREPARATION OF GREEN NANOCATALYST

The green Cu-Mn/TiO_2 nanocatalyst was synthesized using orange peel extract as a bio-reducing and stabilizing agent, along with high-purity titanium, copper, and manganese salts as precursors.

2.12.1. Extraction of orange peel

Fresh orange peels were sourced from local fruit vendors, thoroughly washed to remove impurities, and air-dried under laboratory conditions for approximately seven days. The dried peels were ground into a fine powder using a mortar and pestle. A 20 g portion of this powder was placed into the porous thimble of a Soxhlet extractor. An ethanol-water mixture (120 ml ethanol and 30 ml distilled water; v/v 4:1) was placed in the round-bottom flask, and extraction was conducted at 78 ˚C for 6 h until a clear extract was obtained in the extraction column. The collected extract was transferred into a clean beaker and concentrated on a hot plate at 100 ˚C to remove residual solvents. The concentrated extract was stored for subsequent nanocatalyst synthesis [22].

2.12.2. Synthesis of green Cu-Mn/TiO_2 nanocatalyst

The synthesis procedure followed the method reported by Sahu et al. [22] with slight modifications. Stock solutions of 0.15 M $Ti(NO_3)_4$ (anhydrous), $Mn(CH_3COO)_2{\cdot}4H_2O$ (hydrated), and $Cu(NO_3)_2{\cdot}2.5H_2O$ (hydrated) were prepared separately. A mixture containing 50 ml of $Ti(NO_3)_4$ and 25 ml each of $Mn(CH_3COO)_2{\cdot}4H_2O$ and $Cu(NO_3)_2{\cdot}2.5H_2O$ was combined with 25 ml of the prepared orange peel extract. The solution was stirred magnetically at an elevated temperature (70 °C) for 30 min. Subsequently, 0.1 M NaOH was added dropwise until a pale yellow precipitate formed and a pH of 11 was achieved. The precipitate was separated via centrifugation at 4000 rpm for 20 min, followed by repeated washing with distilled water until a neutral pH was achieved. The product was oven-dried at 80 ˚C for 3 h and then calcined at 550 ˚C for an additional 2 h in a tube furnace under nitrogen as an inert atmosphere. The resulting catalyst was stored in an airtight container for characterization and application. A schematic of the redox sequence showing the chemistry and mechanism of the catalyst synthesis and the stoichiometry of the precipitate formation upon dropwise addition of NaOH to pH 11 are shown in Scheme 1 and equation (13), respectively.

$$\begin{aligned} Ti(NO_3)_4 + 4NaOH &\rightarrow Ti(OH)_4 \downarrow + 4NaNO_3 \\ Cu(NO_3)_2 + 2NaOH &\rightarrow Cu(OH)_2 \downarrow + 2NaNO_3 \\ Mn(CH_3COO)_2 + 2NaOH &\rightarrow Mn(OH)_2 \downarrow + 2CH_3COONa \end{aligned} \quad (13)$$

2.13. CHARACTERIZATION OF GREEN CU-MN/TIO_2 NANOCATALYST

The structural, morphological, and surface properties of the synthesized green Cu-Mn/TO_2 nanocatalyst were characterized using X-ray diffraction (XRD), Fourier-transform infrared spectroscopy (FTIR), scanning electron microscopy (SEM), and

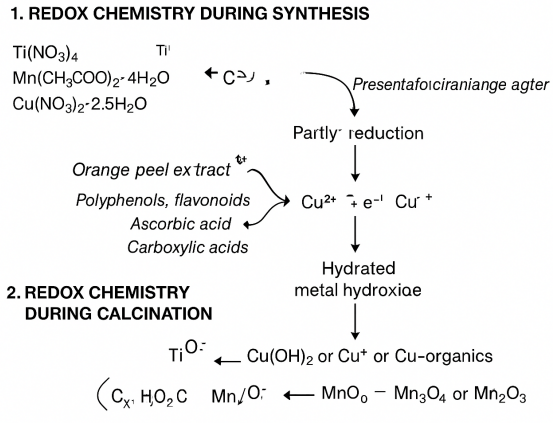

Scheme 1. A schematic of the redox sequence of the chemistry and mechanism involved in the synthesis of the green Cu-Mn/TO_2 nanocatalyst.

Brunauer-Emmett-Teller (BET) surface area analysis, following the procedures outlined in previous studies [22–24].

2.13.1. XRD analysis

XRD patterns were recorded using an X-ray diffractometer (Shimadzu XRD-6000, Japan) operated at 30 kV and 30 mA with CuKα radiation (λ = 0.1541 nm). Thus, A 500 mg sample was evenly pressed onto the XRD plate and subjected to the X-ray diffractometer for analysis after calibration of the instrument. Scans were conducted over a 2θ range of 10˚-80˚. Phase identification was carried out by matching diffraction peaks with the Joint Committee on Powder Diffraction Standards (JCPDS) database.

2.13.2. FTIR analysis

FTIR spectra were obtained using FTIR spectrometer (PerkinElmer Spectrum 100, Waltham, MA, USA) in the range of 4000-500 cm^{-1}. The catalyst sample (5.0 mg) was prepared for FTIR analysis using the KBr pellet technique. The powder was first oven-dried at 100 ˚C for 2 h and cooled in a desiccator to remove adsorbed moisture. To make a ~1% w/w pellet, 5.0 mg of dried catalyst was mixed with 495 mg of spectroscopic-grade KBr. The mixture was ground thoroughly in an agate mortar until it was homogeneous and free-flowing, then transferred to a clean pellet die and compressed at 10 tonnes of pressure for approximately 2 min to form a transparent pellet. A background spectrum was recorded with a pure KBr pellet before sample measurement. The sample pellet was scanned on an FTIR spectrometer over 4000-500 cm^{-1} with a resolution of 4 cm^{-1}. Spectra were baseline corrected and normalized as needed, and characteristic bands were identified and assigned by comparison with reference spectra.

2.13.3. BET surface area measurement

Brunauer-Emmett-Teller (BET) is a gas adsorption technique used to measure the specific surface area and porosity of solid materials through gas adsorption. BET was carried out using an N_2 adsorption/desorption analyzer (Thermo-Finnigan Sormatic 1990 series). The nanocatalyst sample (Cu-Mn/TiO_2) was de-

gassed before use at 150 °C for 24 h to remove the moisture and impurities from the catalyst surface. Then the Adsorption and desorption process of N_2 on the catalyst surface were analyzed in a vacuum chamber at -196 °C. The surface area, total pore volume, and average pore diameter were calculated from the adsorption data.

2.13.4. SEM analysis

The microstructure morphology of the synthesized green Cu-Mn/TiO_2 nanocatalyst was obtained through scanning electron microscopy (SEM) using SEM instrument (JOEL, JSM-6480A, Japan) operated at 20 kV. The sample was mounted on SEM stubs covered with conductive carbon tape, evenly dusted with the catalyst powder (sample), and gold-coated to enhance conductivity before imaging. The SEM stub was transferred into the sample holder for imaging.

2.14. PRE-TREATMENT OF OIL THROUGH ACID ESTERIFICATION

Before transesterification, the extracted oil was pretreated to reduce mainly the free fatty acids (0.96%). Thus, 10 ml of the oil each was dehydrated by heating it above 100 °C on a hot plate to evaporate the water content. The dehydrated oil was then esterified by agitating it with a mixture of methanol (5 ml) and a catalyst (1% H_2SO_4) with the oil in a 100 ml beaker placed on a magnetic hot plate with constant agitation and equipped with a thermometer. The oil was heated to 60 °C and allowed to run for 2 h. The mixture was allowed to settle in a separating funnel into two layers at the end of the reaction time. The upper layer contained methanol and water, while the lower layer contained the oil. The oil was carefully removed from the funnel. The FFA was determined by a standard acid-base titration method using a standard solution of 1.0 M NaOH [11]. This was kept for the transesterification reaction.

2.15. EXPERIMENTAL DESIGN

Biodiesel production from black date seed kernel oil was optimized using a Central Composite Design (CCD) within the framework of Response Surface Methodology (RSM), implemented via Design-Expert 13 software. This approach was employed to determine the optimal operating conditions and to assess the interactive effects of the process parameters on biodiesel yield [18, 23]. The design consisted of four independent variables at five coded levels: $-\alpha$, 1, 0, +1, and $+\alpha$, corresponding to the extreme low, low, central, high, and extreme high levels, respectively (Table 1). In total, the software generated 30 experimental runs. The independent variables were methanol-to-oil molar ratio (X_1, 3-15), catalyst concentration (X_2, 1-5 wt%), reaction temperature (X_3, 35-75 ˚C), and reaction time (X_4, 30-90 min), as outlined in Table 1.

2.16. EXPERIMENTAL PROCEDURE VIA TRANSESTERIFICATION

The biodiesel synthesis from *Canarium schweinfurthii* oil using a green-synthesized Cu-Mn/TiO_2 nanocatalyst was carried out through a transesterification process, following the procedure described by Aqueel et al. [25] with minor adjustments. A 250 ml beaker containing methanol, oil, and the catalyst was placed on a magnetic hot plate, which provided both controlled heating and agitation at 350 rpm to ensure uniform temperature distribution and effective mixing. Reactions were conducted under various conditions as defined by the CCD design matrix (Table 1). Upon completion, the biodiesel was separated and purified according to the standard analytical method reported by Godswill et al. [26].

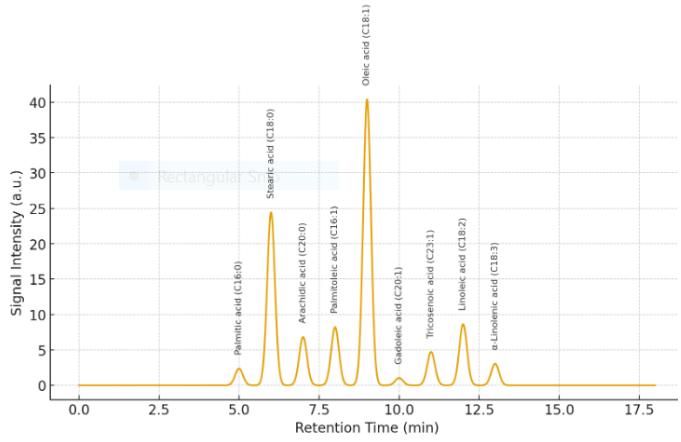

Figure 2. Chromatogram peaks of the fatty acids profile obtained from the GC-MS.

2.17. STATISTICAL DATA ANALYSIS

The experimental data obtained in this study were statistically evaluated using analysis of variance (ANOVA) in Design-Expert 13 software. ANOVA was applied to determine the significance of individual variables, their mutual interactions, and their combined influence on the response. The statistical evaluation involved three key tests: the lack-of-fit test, regression model analysis, and assessment of the significance of model terms. These tests collectively ensured the accuracy, reliability, and predictive strength of the developed model. Furthermore, a second-order polynomial equation was established to mathematically represent the experimental conditions and predict the corresponding responses, as presented in Eq. (14).

$$Y = \beta_0 + \sum_{i=1}^{k} \beta_i x_i + \sum_{i=1}^{k} \beta_{ii} x_i^2 + \sum_{1 \le i \le j}^{k} \beta_{ij} x_i x_j + C, \qquad (14)$$

where Y is the response (%); β_0, β_i, β_{ii}, and β_{ij} are the intercept, linear, quadratic, and interaction coefficients, respectively, while X_i and X_j are the independent factors.

3. RESULTS AND DISCUSSION

3.1. CHARACTERIZATION OF THE EXTRACTED BLACK DATE OIL

The physicochemical characteristics of *Canarium schweinfurthii* seed kernel oil were evaluated to determine its potential for biodiesel production. The parameters analyzed included oil yield, density, viscosity, moisture content, sulfur content, iodine value (IV), free fatty acid (FFA) content, peroxide value (PV), acid value (AV), and saponification value (SV), as summarized in Table 2. From an economic perspective, feedstock availability is the most critical factor influencing biodiesel production cost, accounting for nearly 80% of the total expense [27, 28].

Table 1. Central Composite Design (CCD) with coded and actual values of experimental parameters of the design matrix used in the production of biodiesel for all the samples.

Independent variables	Symbols	Coded levels				
		-α	-1	0	1	+α
Methanol to oil molar ratio (mol)	X_1	3:1	6:1	9:1	12:1	15:1
Catalyst concentration (wt.%)	X_2	1.0	2.0	3.0	4.0	5.0
Temperature (˚C)	X_3	35.0	45.0	55.0	65.0	75.0
Time of reaction (min)	X_4	30.0	45.0	60.0	75.0	90.0

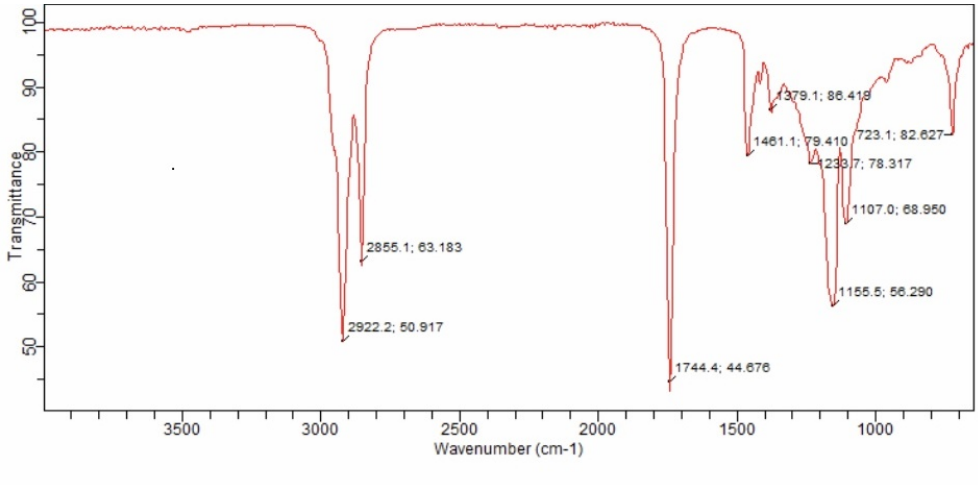

Figure 3. FTIR spectra of green synthesized Cu-Mn/TiO_2 nano catalyst.

Table 2. Physicochemical properties of extracted oil from black date (*Canarium schweinfurtii*) seed kernel sample.

Parameters	Black date seed oil
Yield (wt%)	49.12 ± 2.14
Density (kg/m^3)	935.60 ± 4.02
Viscosity@40 ˚C (mm^2/s)	1.97 ± 0.11
Moisture (%)	0.81 ± 0.20
Sulphur (ppm)	ND
Iodine value (mg g^{-1})	107.40 ± 3.13
Free fatty acid (%)	1.32 ± 0.01
Peroxide value (meq/kg)	11.80 ± 0.68
acid value (mgKOH/g)	3.56 ± 0.14
Saponification value (mgKOH/g)	216.56 ± 1.89

ND; not detected

Table 3. Fatty acid profiles of black date (*Canarium schweinfurtii*) seed kernel oil.

Fatty acid (%)	MW (g/mol)	Formula	Composition (%)
Lauric acid (C12:0)	200	$C_{12}H_{24}O_2$	ND
Palmitic acid (C16:0)	256	$C_{16}H_{32}O_2$	2.36
Stearic acid (C18:0)	284	$C_{18}H_{36}O_2$	24.42
Arachidic acid (C20:0)	312	$C_{20}H_{40}O_2$	6.81
Palmitoleic (C16:1)	254	$C_{16}H_{30}O_2$	8.21
Oleic acid (C18:1)	282	$C_{18}H_{34}O_2$	40.42
Gadoleic (C20:1)	310	$C_{20}H_{38}O_2$	1.03
Tricosenoic acid (C23:1)	322	$C_{23}H_{44}O_2$	4.70
Linoleic acid (C18:2)	280	$C_{18}H_{32}O_2$	8.62
α-Linolenic acid (C18:3)	278	$C_{18}H_{30}O_2$	3.05

MW: molecular weight, ND: not detected

In this study, the *Canarium schweinfurthii* seeds yielded 49.12 ± 2.14% oil, indicating a promising biodiesel feedstock. This result

Table 4. Summary of the crystallite size estimates of the synthesized green Cu-Mn/TiO_2 nanocatalyst.

2θ (˚)	FWHM β (rad)	Crystallite Size (nm)
25.12	0.00454	31.30
34.82	0.00384	32.02
40.54	0.00419	32.57
43.10	0.00838	32.84
62.40	0.00676	35.71

Table 5. Textural properties of the synthesized green Cu-Mn/TiO_2 nanocatalyst compared to similar literature catalysts.

Catalyst	BET area (m^2 g^{-1})	Pore volume (cm^3 g^{-1})	Average pore diameter (nm)
Cu-Mn/TiO_2 (This work)	24.502	0.01048	5.28
CaO-TiO_2 [37]	40.34	0.14	6.10
Mn/TiO_2 [38]	50.90	0.22	5.03

closely aligns with the 50.1% yield reported for African black olive seed (*Canarium schweinfurthii*) by Cordelia *et al.* [16] and the 49.80% obtained by Muhammad *et al.* [21]. Such variations in yield for similar seed types may be attributed to differences in environmental conditions or experimental procedures.

Biodiesel generally exhibits higher density and lower compressibility compared to petroleum diesel, which can limit its di-

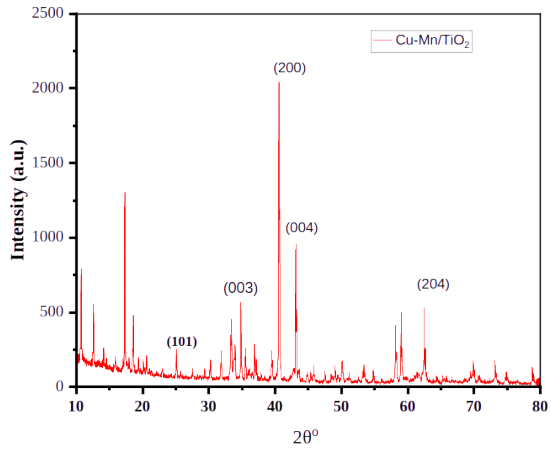

Figure 4. X-ray diffraction spectra of green synthesized Cu-Mn/TiO_2 nano catalyst.

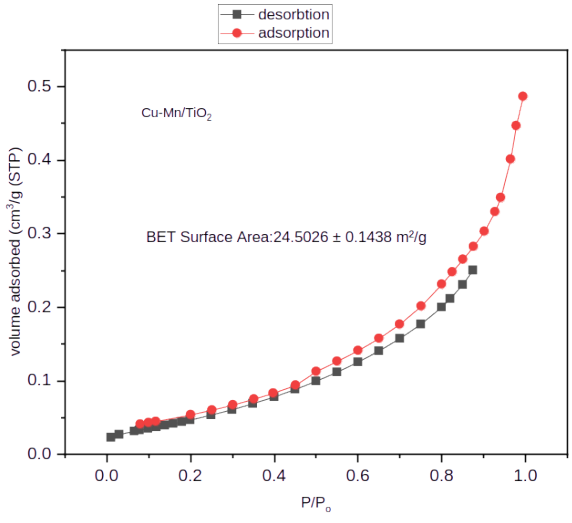

Figure 5. BET surface area analysis of green-synthesized Cu-Mn/TiO_2 nano catalyst.

rect use in engines [14, 28]. According to ASTM specifications, ideal biodiesel densities range between 860-900 kg/m^3. The density of African black olive seed oil in this study was 935.60 ± 4.02 kg/m^3, which falls slightly above the recommended range but is still considered acceptable for biodiesel production. Comparable density values have been reported, ranging from 830 kg/m^3 in mango seed oil to 936 kg/m^3 in African black [16, 25, 26]. Viscosity, a critical property influencing fuel atomization and combustion, was found to be 1.97 ± 0.11 mm^2/s within the ASTM D6751 standard range of 1.9-6.0 mm^2/s, indicating good suitability for biodiesel production. Moisture content, recorded at 0.81 ± 0.20%, was well below the ASTM D5744 limit of 8 ± 1.3%, minimizing the risk of soap formation and gelation during transesterification [28]. Sulfur, which contributes to harmful SOx emissions, was not detected in the sample, indicating low environmental impact potential from sulfur-related emissions.

The iodine value, which reflects the degree of unsaturation in

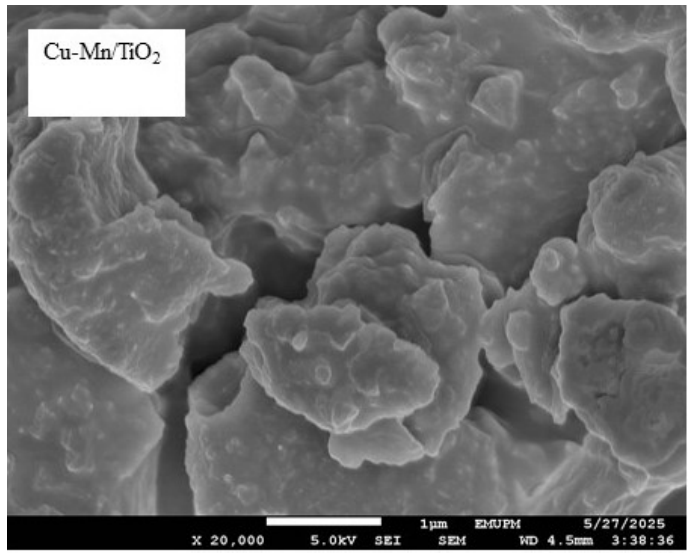

Figure 6. SEM micrograph of green-synthesized Cu-Mn/TiO_2 nano catalyst.

Table 6. Experimental design (CCD) matrix, the actual and predicted values of the biodiesel yield produced from black date seed kernel oil using Cu-Mn/TiO_2 nanocatalyst.

No. of runs	X_1	X_2	X_3	X_4	Experimental yield (%)	Predicted yield (%)
1	9:1	3.0	55.0	60.0	84.42	84.62
2	9:1	5.0	55.0	60.0	86.96	86.96
3	6:1	2.0	65.0	45.0	85.79	85.34
4	3:1	3.0	55.0	60.0	86.06	86.48
5	12:1	4.0	65.0	45.0	86.96	86.96
6	6:1	2.0	45.0	75.0	83.18	82.65
7	9:1	3.0	55.0	60.0	90.16	89.67
8	6:1	4.0	45.0	75.0	88.33	87.64
9	9:1	1.0	55.0	60.0	81.81	81.86
10	9:1	3.0	55.0	30.0	85.58	85.19
11	12:1	4.0	45.0	75.0	85.54	85.44
12	6:1	2.0	65.0	75.0	86.96	86.96
13	6:1	4.0	65.0	30.0	88.73	88.95
14	9:1	3.0	55.0	60.0	88.77	88.69
15	9:1	3.0	55.0	90.0	84.20	83.88
16	12:1	4.0	65.0	75.0	84.02	84.43
17	9:1	3.0	55.0	60.0	77.44	77.62
18	12:1	2.0	65.0	45.0	82.49	83.15
19	12:1	2.0	45.0	45.0	84.68	84.74
20	15:1	3.0	55.0	60.0	86.96	86.96
21	9:1	3.0	75.0	60.0	83.36	84.12
22	12:1	2.0	45.0	75.0	86.71	86.85
23	6:1	4.0	45.0	45.0	85.34	85.58
24	12:1	4.0	45.0	45.0	86.96	86.96
25	6:1	2.0	45.0	45.0	86.96	86.96
26	12:1	2.0	65.0	75.0	95.07	95.22
27	9:1	3.0	55.0	60.0	89.67	89.65
28	9:1	3.0	55.0	60.0	81.67	81.62
29	6:1	4.0	65.0	75.0	82.34	82.49
30	9:1	3.0	35.0	60.0	78.50	77.98

Note: X_1: methanol to oil ratio, X_2: catalyst concentration (wt%), X_3: temperature (°C), and X_4: reaction time (min).

oils, was 107.4 ± 3.13 mg/g within the ASTM limit of < 120 mg/g. This value, consistent with Cordelia *et al.* [16] (108 mg/g), suggests good cold-flow performance but a higher sus-

Table 7. ANOVA and fit statistics results obtained from the quadratic model for biodiesel production from the black date seed kernel oil.

Source	Sum of Squares	Degree of freedom	Mean Square	F-value	p-value (0.05/95% CL)
Model	348.11	14	24.87	111.03	< 0.0001 Significant
A-Methanol to oil	0.73	1	0.73	3.27	0.0908
B-Catalyst concentration	30.26	1	30.26	135.13	< 0.0001
C-Temperature	69.94	1	69.94	312.29	< 0.0001
D-Reaction time	1.23	1	1.23	5.49	0.0334
AB	2.36	1	2.36	10.56	0.0054
AC	33.79	1	33.79	150.86	< 0.0001
AD	89.07	1	89.07	397.69	< 0.0001
BC	69.60	1	69.60	310.76	< 0.0001
BD	32.46	1	32.46	144.95	< 0.0001
CD	2.85	1	2.85	12.72	0.0028
A^2	5.98	1	5.98	26.71	0.0001
B^2	4.21	1	4.21	18.82	0.0006
C^2	4.88	1	4.88	21.81	0.0003
D^2	7.37	1	7.37	32.89	< 0.0001
Residual	3.36	15	0.22		
Lack of Fit	2.74	10	0.34	2.71	0.1230 Not significant
Pure Error	0.62	5	0.12		
Cor Total	351.47	29			

Std. Dev. = 0.47, Mean = 85.52, C.V. % = 0.55, R^2 = 0.99, Adjusted R^2 = 0.98, Predicted R^2 = 0.94, Adeq Precision = 52.62
Note: A = X_1: methanol to oil ratio, B = X_2: catalyst concentration (wt%), C = X_3: temperature (°C) and D = X_4: reaction time (min).

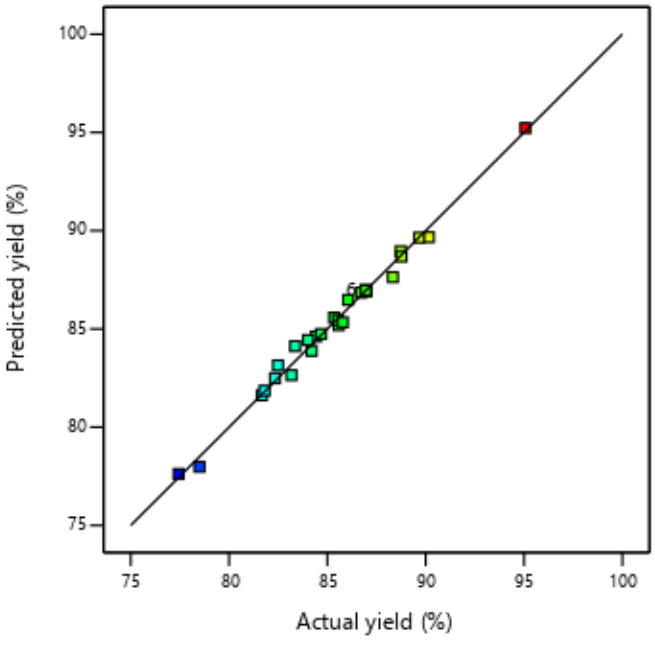

Figure 7. Experimental yield against predicted yield for the biodiesel produced from black date seed oil.

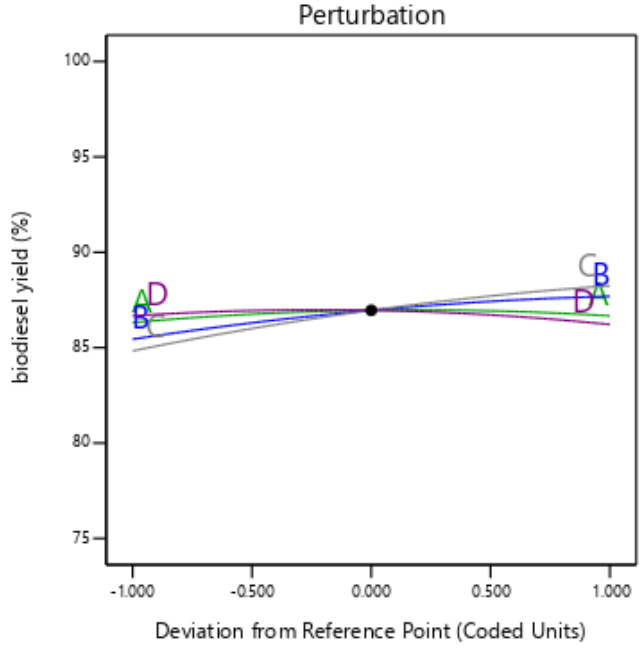

Figure 8. Effect of process parameters on biodiesel production from black date seed oil (A = X_1: methanol to oil ratio, B = X_2: catalyst concentration (wt%), C = X_3: temperature (°C), and D = X_4: reaction time (min)).

ceptibility to oxidative degradation [27, 28]. The FFA content was 1.32 ± 0.01%, slightly exceeding the 1% threshold beyond which pretreatment is recommended [18, 29, 30], implying that pre-esterification may be necessary before biodiesel synthesis. Peroxide value, an indicator of oxidative stability, was 11.80 ± 0.68 meq O_2/kg slightly higher than the recommended < 10 meq O_2/kg suggesting a higher risk of rancidity during storage [29]. The acid value was 3.56 ± 0.14 mg KOH/g, notably lower than the 12.6 mg KOH/g reported for similar oils by Cordelia *et al.* [16], possibly due to differences in handling or processing conditions. Finally, the saponification value was 216.56 ± 1.89 mg KOH/g, indicating a predominance of short-chain fatty acids, which can enhance biodiesel volatility and combustion efficiency [30].

3.2. ANALYSIS OF FATTY ACID PROFILE OF THE BLACK DATE OIL

The fatty acid composition of an oil is a critical factor in determining its performance as a biodiesel feedstock, as it directly in-

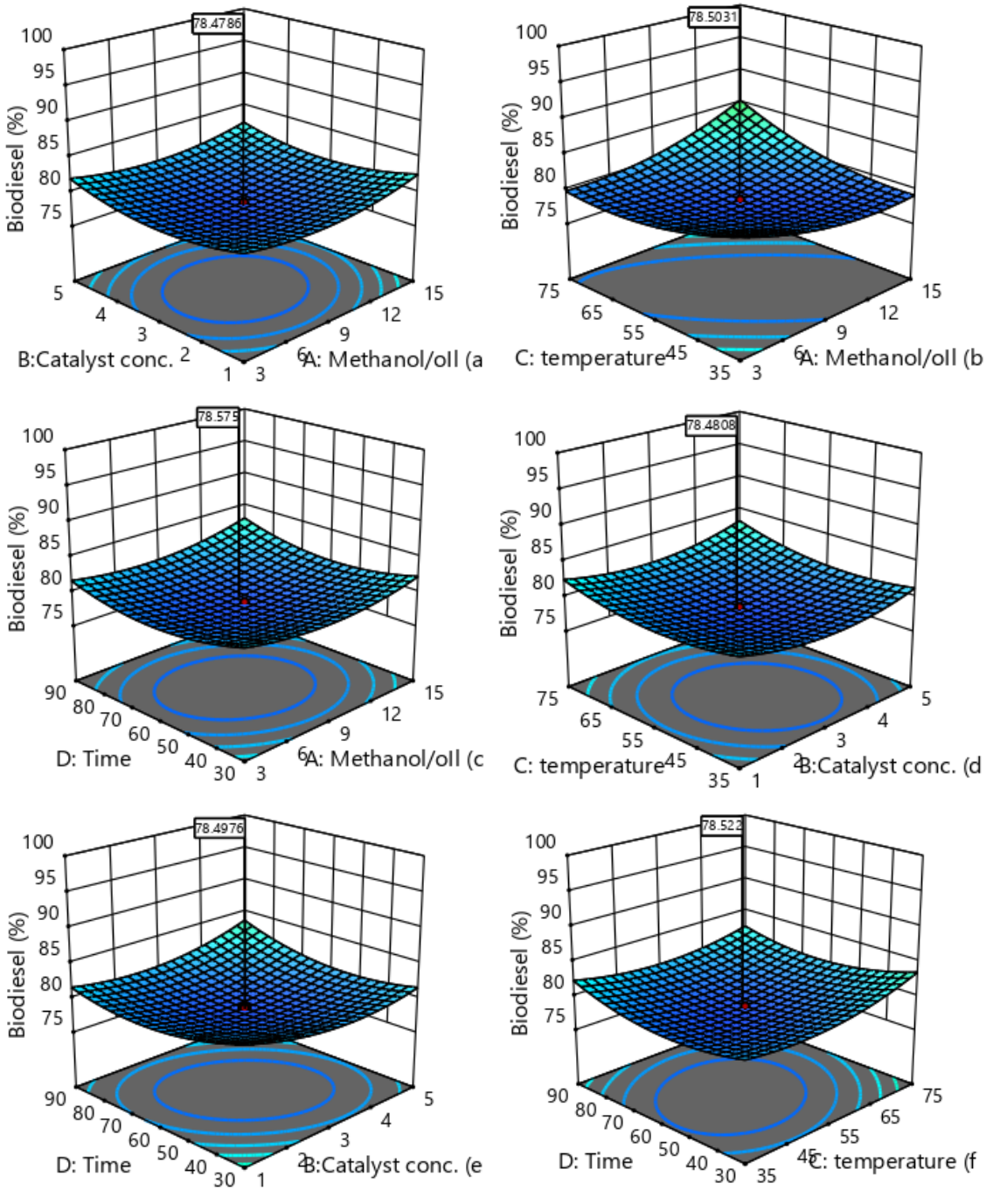

Figure 9. 3D plots showing the effects of (a) methanol/oil molar ratio against catalyst concentration (wt%), (b) temperature (°C) against methanol/oil molar ratio, (c) reaction time (min) against methanol/oil molar ratio, (d) temperature (°C) against catalyst concentration (wt%), (e) reaction time (min) against catalyst concentration (wt%), and (f) reaction time (min) against temperature (°C) on the biodiesel yield produced from black date seed oil.

fluences oxidative stability, cold-flow characteristics, and cetane number. The fatty acid distribution of *Canarium schweinfurthii* seed kernel oil is presented in Table 3 and depicted in Figure 2. The analysis revealed the presence of saturated fatty acids (SFAs), including palmitic, stearic, and arachidic acids, as well as monounsaturated fatty acids (MUFAs) such as oleic and palmitoleic acids, and polyunsaturated fatty acids (PUFAs), including linoleic and α-linolenic acids. In total, nine distinct fatty acids were identified, with SFAs accounting for 33.59%, MUFAs for 54.36%, and PUFAs for 11.67%. Overall, the proportion of unsaturated fatty acids reached 66.03%, indicating a highly unsaturated oil profile typical of feedstocks favorable for biodiesel production [20, 21]. Among the SFAs, stearic acid (24.42%) and arachidic acid (6.81%) were predominant, while palmitic acid was present at a relatively low level (2.36%), and lauric acid was absent. The MUFA fraction was dominated by oleic acid (40.42%), whereas the PUFA fraction was largely composed of linoleic acid (8.62%). Literature confirmed that high SFA content enhances oxidative stability and cetane number but tends to compromise cold-flow performance, whereas high PUFA con-

Table 8. Physicochemical properties of biodiesel produced from Africana black date seed kernel oil using green-synthesized Cu-Mn/TiO_2 nano catalyst and ASTM standards.

Parameters	Black date seed	ASTM D6751 Standard
Density (kg/m^3)	885.00 ± 2.31	860-900
Specific gravity	0.88 ± 0.14	0.8-0.9
viscosity@ 40 ˚C (mm^2/s)	5.25 ± 1.04	1.9 – 6.0
Moisture (%)	0.77 ± 0.11	≤ 0.05
Pour point (˚C)	3.20 ± 0.17	-5-10
Flash point (˚C)	144.10 ± 1.43	≥130
Sulphur (ppm)	ND	0.002
Iodine value (mg g^{-1})	44.53 ± 2.32	≤120
Oxidative stability (h)	6.10 ± 1.05	3-4
Acid value (mgKOH/g)	0.21 ± 0.72	0.1-0.5
Saponification value (mgKOH/g)	167.30 ± 4.31	≤370
Calorific value (MJ/kg)	56.60 ± 1.04	37-41
Cetene number (min)	53.25 ± 2.79	48-65

ND: not detected

tent improves cold-flow properties but reduces oxidative stability [21, 31].

Based on this composition, the studied oil is expected to exhibit strong oxidative stability due to its high stearic and oleic acid content, although this stability could be marginally diminished by the level of linoleic acid in the study. The cetane number is likely to be excellent, with cold-flow performance expected to be moderate. These findings are consistent with those reported by Chomini *et al.* [31] and Marcos *et al.* [32] for black date and avocado seed kernel oils. However, they contrast with earlier reports for orange seed oil, avocado oil, and even prior studies on African black olive seed oil [16, 33]. Such discrepancies may be attributed to differences in seed variety, environmental growing conditions, or variations in extraction and analytical procedures.

3.3. CHARACTERIZATION OF THE SYNTHESIZED GREEN NANO CATALYST

3.3.1. FTIR analysis

The FTIR spectrum of the green-synthesized Cu-Mn/TiO_2 nanocatalyst, produced using orange peel extract, displayed distinct absorption bands that signified the presence of both organic biomolecules and metal-oxygen linkages (Figure 3). These spectral patterns reflect surface functional groups and confirm that bioactive plant-derived molecules were successfully incorporated during synthesis. A broad peak around 3430 cm^{-1} was assigned to O-H stretching vibrations originating from hydroxyl groups in alcohols, phenols, and possibly adsorbed moisture. The width and intensity of this peak indicate strong hydrogen bonding, consistent with polyphenolic compounds from the orange peel extract. A weaker absorption at approximately 2920 cm^{-1} corresponds to aliphatic C-H stretching in -CH_2 and -CH_3 groups, implying the presence of flavonoids or terpenoids, which act as natural reducing and stabilizing agents during nanoparticle formation. The band at 1620 cm^{-1} was attributed to C=O stretching or aromatic C=C vibrations, suggesting the presence of carbonyl groups and lignin-like aromatic structures involved in surface modification and metal chelation. The absorption near 1380 cm^{-1} likely corresponds to C-N stretching or O-H bending, pointing to residual amines or carboxylic groups from plant metabolites. A prominent feature at 1100 cm^{-1} was linked to C–O stretching in alcohols, ethers, or esters, supporting the role of organic compounds as capping agents. Additionally, strong absorptions below 700 cm^{-1}, particularly within 530-570 cm^{-1}, were characteristic of Ti-O, Cu-O, and Mn-O stretching vibrations, confirming the formation of mixed metal oxides anchored on the TiO_2 support. The coexistence of organic and inorganic signals indicates strong surface functionalization, which enhances catalyst stability, dispersion, and reactivity in environmental and energy conversion processes [22].

3.3.2. X-ray diffraction (XRD) analysis

The X-ray diffraction pattern of the green Cu-Mn/TiO_2 nanocatalyst prepared via a green synthesis route (Figure 4) displayed sharp and well-resolved diffraction peaks, indicating a highly crystalline material. Anatase TiO_2 was identified as the predominant phase, with the strongest diffraction peak appearing at $2\theta \approx 25.1^{\circ}$, corresponding to the (101) crystallographic plane of tetragonal anatase TiO_2 (JCPDS No. 21-1272). The retention of this phase confirms that the catalytically favorable anatase structure remained stable after the introduction of Cu and Mn species. A noticeable shift of the (101) reflection toward lower diffraction angles compared with pristine anatase TiO_2 ($2\theta \approx 25.3^{\circ}$) was observed, which can be ascribed to lattice distortion and microstrain arising from the substitution of Ti^{4+} by Cu^{2+}/Cu^{+} and Mn^{2+}/Mn^{3+} ions, as well as enhanced metal–support interactions promoted by the green synthesis process. Such diffraction peak shifts are frequently reported for doped TiO_2 systems and provide evidence of successful metal incorporation without altering the anatase phase [40]. Additional reflections located at $2\theta \approx 34.82^{\circ}$, 40.54°, 43.10° and 62.40° were assigned to the (103), (200), (004), and (204) planes of anatase TiO_2, respectively, further confirming the preservation of the tetragonal crystal structure. No distinct diffraction peaks attributable to crystalline CuO, Cu_2O, metallic Cu, or manganese oxide phases were detected, suggesting that the incorporated Cu and Mn species are either uniformly dispersed on the TiO_2 surface or exist in an amorphous or ultra-fine nanocrystalline state below the detection limit of XRD. Such high dispersion is desirable for catalytic applications, as it enhances the accessibility of active sites while maintaining the structural stability of the TiO_2 support [34].

Furthermore, the crystallite size estimates of the green Cu-Mn/TiO_2 nanocatalyst were determined (Table 4) using the Scherrer equation based on the anatase (101), (103), (200), (004), and (204) reflections, yielding an average value of approximately 32.9 nm, indicative of a nanocrystalline material. The presence of sharp and well-resolved diffraction peaks reflects the high crystallinity of the anatase TiO_2 phase following metal incorporation and is consistent with the growth-controlling and stabilizing effects of phytochemicals involved in the green synthesis process [35]. The lattice parameters calculated from the anatase reflections were a = b = 3.78 Å and c = 9.49 Å, closely matching the standard values for anatase TiO_2. This indicates that Cu–Mn incorporation caused only minor lattice expansion without disrupting the overall tetragonal framework [36].

3.3.3. Brunauer-Emmett-Teller (BET) surface area analysis

The BET analysis of the Cu-Mn/TiO_2 nanocatalyst revealed a Type IV nitrogen adsorption-desorption isotherm with an H3 hysteresis loop (Figure 5), characteristic of mesoporous materi-

als according to IUPAC classification. The pore size distribution ranged from 2-50 nm, with slit-shaped pores resulting from agglomerated plate-like structures or loosely packed particles. In addition, the nanocatalyst exhibits a BET surface area of 24.5 m^2/g, a pore volume of 0.0105 cm^3/g, and an average pore diameter of 5.28 nm derived from BJH desorption analysis (Table 5). Although its surface area is lower than the mixed-oxide catalysts reported in Table 5 obtained from the literature [37, 38], the pore diameter lies within the mesoporous range, which is critical for transesterification involving bulky triglyceride molecules [38]. Furthermore, in heterogeneous catalysis, pore accessibility and diffusion efficiency are often more influential than exceptionally high surface area [36, 37]. The mesoporous structure of Cu-Mn/TiO_2 facilitates effective diffusion of reactants while maintaining adequate exposure of active sites. Furthermore, strong metal–support interactions enhance structural stability, making the catalyst suitable for efficient heterogeneous transesterification [36].

3.3.4. Scanning electron microscopy (SEM) analysis

SEM imaging revealed a granular and heterogeneous surface morphology (Figure 6). The particles appeared nanosized (20-50 nm), mostly spherical to oval in shape, and were distributed unevenly across the TiO_2 support. Agglomeration was visible, likely due to drying and synthesis conditions, but individual particle boundaries remained identifiable. The irregular surface texture and nanoscale structure increase the available surface area, aligning with BET results. This morphology is advantageous for catalysis, as it provides abundant active sites and facilitates efficient reactant-catalyst contact, making the material promising for thermochemical applications such as gasification and biodiesel production [22].

3.4. DATA ANALYSIS OF THE PRODUCED BIODIESEL

Biodiesel production from black date seed oil was optimized using a Central Composite Design (CCD) experimental framework, with a green-synthesized nanocatalyst as the active material. The optimization results (Tables 6 and 7) demonstrated that the selected process variables had a pronounced effect on biodiesel yield, with predicted and experimental values ranging from 77.62-95.22% and 77.44-95.07%, respectively. The maximum yield was achieved in Run 26 under the following conditions: methanol-to-oil molar ratio of 12:1, catalyst loading of 2 wt%, reaction temperature of 65 ˚C, and reaction time of 75 minutes. These results confirm that the nanocatalyst enabled highly efficient transesterification when operated under optimal parameters.

When compared to literature reports, the highest yield obtained in this study exceeded the 87.25% reported by Sunjurjo *et al.* [39] for biodiesel production from *Nannochloropsis gaditana* under optimized conditions (methanol-to-oil ratio 12:1, temperature 50 ˚C, reaction time 67.5 minutes). However, it was slightly lower than the 98.04% yield reported by Natália *et al.* [40] for palm oil biodiesel synthesized with a natural coconut-oil-based surfactant (reaction time 30 minutes, potassium hydroxide 1 wt%, methanol-to-oil ratio 8.28:1, surfactant 1.05 wt%). The differences in yield across studies are likely due to variations in feedstock composition, reaction conditions, and catalyst characteristics.

Statistical evaluation using ANOVA (Table 7) confirmed the robustness of the developed quadratic regression model, which yielded an F-value of 111.03 and a p-value < 0.0001, indicating high model significance. The model also exhibited excellent predictive accuracy, as evidenced by a high coefficient of determination (R^2 = 0.9904), adjusted R^2 = 0.9815, and predicted R^2 = 0.9449. The lack-of-fit test returned a p-value of 0.123 (> 0.05), confirming that the model reliably represented the experimental data. A parity plot (Figure 7) further demonstrated the strong agreement between predicted and actual yields.

The empirical relationship between the coded variables and biodiesel yield (%) is as:

$$\begin{aligned} Y &= 86.96 + 0.174583A + 1.12292B + 1.70708C - 0.22625D \\ &\quad + 0.384375AB + 1.45313AC + 2.35938AD + 2.08563BC \\ &\quad + 1.42438BD - 0.421875CD - 0.466979A^2 \\ &\quad - 0.391979B^2 - 0.421979C^2 - 0.518229D^2. \end{aligned} \tag{15}$$

Here, negative coefficients (e.g., for reaction time D, the temperature-time interaction CD, and all quadratic terms) indicate that increasing these variables beyond optimal values reduces yield. Positive coefficients suggest a beneficial effect on yield up to a certain limit.

The perturbation plot (Figure 8) revealed that each parameter followed a pattern of initial yield improvement followed by a decline at higher levels. Temperature had the most significant individual influence, as confirmed by ANOVA (F = 312.29, p < 0.05). Catalyst concentration and reaction time also showed strong effects, while the methanol-to-oil ratio alone was not statistically significant (p = 0.0908) but had important synergistic interactions, especially with temperature and time.

For the combined effects, Figure 9 presents six 3D surface plots illustrating the interactive effects of two transesterification parameters on biodiesel yield from black date seed kernel oil, while keeping the remaining parameters constant. The biodiesel yield in the plots ranged from approximately 65% to 94%, depending on the parameter combinations. The effect of the interaction between methanol-to-oil molar ratio (A) and catalyst concentration (B) indicated that the yield increased with both methanol-to-oil ratio and catalyst concentration up to an optimal point. Maximum yield (≈92-94%) was observed at around a 6:1 molar ratio and 1.0–1.2 wt% catalyst. Beyond this range, a further increase in the catalyst slightly reduced the yield (Figure 9a). The temperature (C) versus methanol-to-oil molar ratio (A) indicated that the yield improved with increasing temperature and methanol ratio up to the optimum levels. A biodiesel yield of about 93% was achieved at a temperature of 55-60˚C and a 6:1 molar ratio (Figure 9b). The reaction time (D) versus the methanol-to-oil molar ratio (A) indicated that the yield increased with both reaction time and molar ratio, peaking around 60-70 min and a 6:1 molar ratio, where the yield approached 94%. Prolonged reaction times beyond this point showed no substantial gain in yield (Figure 9c). The temperature (C) versus catalyst concentration (B) indicated that the yield improved with increases in both temperature and catalyst concentration. Optimal yield (≈93%) occurred at 55-60˚C and 1.0-1.2 wt% catalyst (Figure 9d). Excessive catalyst or temperature had diminishing

returns. The combined effect of reaction time (D) versus catalyst concentration (B) was shown. An increase in reaction time and catalyst concentration led to increased biodiesel yield, peaking around 70 min and 1.2 wt% catalyst, reaching approximately 92-93% (Figure 9e). Further increases slightly reduced the yield, likely due to saponification. The effect of interaction between reaction time (D) versus temperature (C), which is the last effect in the plots, shows that the yield increased with both parameters up to a certain limit. Maximum yield (≈93-94%) occurred at around 60˚C and 70 min (Figure 9f). Beyond these values, the yield plateaued, suggesting optimal conversion had been reached.

Furthermore, among all interactions, the methanol-to-oil ratio × reaction time (AD) had the strongest effect (F = 397.69), indicating significant synergy between these parameters. Other highly significant interactions included AC, BC, and BD ($p < 0.0001$), consistent with the response surface trends. Additionally, all the quadratic terms (A^2, B^2, C^2, D^2) were found to be statistically significant, confirming the nonlinear nature of the biodiesel production process.

The low coefficient of variation (C.V = 0.5534%), small standard deviation (0.4732), and high adequate precision (52.6150) confirm the reproducibility and robustness of the results. These findings align with Ketema [20], who also reported that all interaction and quadratic terms were statistically significant, underscoring the nonlinear nature of biodiesel production optimization.

3.5. OPTIMIZATION OF PROCESS PARAMETERS AND MODEL VALIDATION

The process parameters were optimized and the model validated using a numerical desirability function within the Central Composite Design (CCD) framework. Optimization was performed by setting the independent variables within their defined ranges, while the response variable (biodiesel yield) was targeted for maximization to achieve the highest possible output. The numerical optimization suggested the following optimal conditions for biodiesel production: catalyst dosage of 2.5 wt%, methanol-to-oil molar ratio of 12.5:1, reaction temperature of 64 ˚C, and reaction time of 60 min. Transesterification was then carried out under these conditions in triplicate, and the obtained results were 95.10%, 95.12% and 95.11% with a mean ± SD of 95.11± 0.01%.

The predicted yield under these optimized conditions was 94.83%, while the average experimentally obtained yield was 95.11± 0.01% resulting in a percentage error of only 0.26%. This error, being well below 1%, confirms both the accuracy of the experimental data and the reliability of the CCD model in optimizing the transesterification process to achieve maximum biodiesel yield.

3.6. CHARACTERIZATION OF THE PRODUCED BIODIESEL

The physicochemical analysis of biodiesel synthesized with the green Cu–Mn/TiO_2 nanocatalyst shows that most properties comply with ASTM D6751 standards (as seen in Table 8), confirming its potential as a diesel alternative. The density (885 kg/m^3) and specific gravity (0.88) fall within the acceptable range, ensuring proper fuel atomization and injection, while the kinematic viscosity (5.25 mm^2/s) supports smooth flow and effective engine lubrication [28]. The moisture content (0.77%) exceeds the ASTM limit (≤0.05%), likely due to residual water in the biodiesel resulting from incomplete drying after separation from the other components (glycerol and catalyst) in the separating funnel, which suggests further drying to remove or reduce the moisture content to the recommended standard, as high moisture content compromise storage stability and engine performance. Thus, high moisture content promotes microbial growth and hydrolysis, leading to the formation of free fatty acids, which can cause corrosion in storage tanks. While in the engine, it can reduce lubricity, cause incomplete combustion, form deposits, and promote injector and fuel system corrosion. It may also reduce fuel efficiency and increase emissions [20, 41]. The pour point (3.2˚C) and flash point (144.1˚C) are within favorable ranges, indicating good low-temperature operability and safe handling. Other parameters, including sulfur (ND), iodine value (44.53 mg/g), oxidative stability (6.1 h), acid value (0.21 mg KOH/g), and saponification value (167.3 mg KOH/g), meet or surpass ASTM requirements, reflecting low corrosivity, moderate unsaturation, and good storage stability.

Furthermore, the produced biodiesel showed a high calorific value of 56.5 MJ/kg, exceeding the ASTM D6751 standard range of 37-41 MJ/kg. However, it is consistent with the 59 MJ/kg reported by Ref. [16] for black dates. This high energy content can be attributed to the chemical composition of the oil, particularly the abundance of long-chain saturated fatty acids in the oil, as well as the effective conversion to fatty acid methyl esters facilitated by the Cu–Mn/TiO_2 nanocatalyst. The elevated calorific value increases the fuel's energy density, potentially enhancing engine performance and efficiency, while remaining suitable for use in diesel engines. The cetane number (53.25 min) indicates efficient ignition performance comparable to conventional diesel [41, 42].

4. CONCLUSION

In conclusion, the CCD-based optimization successfully determined the critical operating parameters for achieving maximum biodiesel yield from black date seed kernel oil using the synthesized green nanocatalysts. The results revealed that both the individual variables and their interactive effects, particularly temperature, catalyst type, and catalyst dosage, played significant roles in the process performance. The validated model offers a dependable basis for scaling up biodiesel production from this non-edible oil source. Overall, the study confirms the potential of black date seed kernel oil as a sustainable, non-edible feedstock for biodiesel production when optimized through statistical modeling and enhanced with appropriate nanocatalysts, thereby contributing to the advancement of renewable fuel alternatives.

DATA AVAILABILITY STATEMENT

The data are available with the corresponding author upon request.

References

[1] B. R. Moser, D. Christina, B. B. Grigo, J. K. Winkler-Moser & M. D. Kenneth, "Production and evaluation of biodiesel from sweet orange (*Citrus sinensis*) lipids extracted from waste seeds from the commercial orange juicing process," Fuel **342** (2023) 1. https://doi.org/10.1016/j.fuel.2023.127727.

[2] M. Rajayokkiam, V. Moorthy & T. K. Kuruba, "Optimization of okra (*Abelmoschus esculentus*) biodiesel production using RSM technique coupled with GA: Addressing its performance and emission characteristics," J. Clean. Prod. **380** (2022) 1. https://doi.org/10.1016/j.jclepro.2022.134870.

[3] T. M. Onyia, P. C. Agu, C. E. Emmanuel & M. C. Onyia, "Optimization of biodiesel production from palm kernel oil using heterogeneous catalyst: Physicochemical characterization and process parameter effects," Int. J. Innov. Sci. Mod. Eng. **12** (2024) 6. https://doi.org/10.35940/ijisme.G1320.1206062.

[4] X. Tan, H. Zhang, H. Li & S. Yang, "Electrovalent bifunctional acid enables heterogeneously catalytic production of biodiesel by (trans)esterification of non-edible oils," Fuel **310** (2022) 122273. https://doi.org/10.1016/j.fuel.2021.122273.

[5] O. U. Igri & U. H. Hyginus, "Effects of process parameters variations and optimization of biodiesel production from orange seed oil using raw and thermal clay as catalyst," Int. J. Front. Eng. Technol. Res. **5** (2023) 1. https://doi.org/10.53294/ijfetr.2023.5.1.0018.

[6] S. K. Kumar & J. Yadav, "A review on bio-based feedstock, synthesis, and chemical modification to enhance tribological properties of biolubricants," Ind. Crops Prod. **193** (2023) 116122. https://doi.org/10.1016/j.indcrop.2022.116122.

[7] K. J. Dipak, B. Samyabrata, P. D. Sudipta & B. Barnali, "The optimization of biodiesel production from waste cooking oil catalyzed by ostrich-eggshell-derived CaO through various machine learning approaches," Cleaner Energy Syst. **3** (2022) 1. https://doi.org/10.1016/j.cles.2022.100033.

[8] IEA, "Task33 International Energy Agency (IEA) Bioenergy Task 33E—Thermal Gasification of Biomass Database," 2018. [Online]. Available: http://task33.ieabioenergy.com/. [Accessed: Feb. 20, 2018].

[9] S. Sahani, T. Roy, Chandra & Y. Sharma, "Clean and efficient production of biodiesel using barium cerate as a heterogeneous catalyst for the biodiesel production; kinetics and thermodynamic study," J. Clean. Prod. **237** (2019) 117699. https://doi.org/10.1016/j.jclepro.2019.117699.

[10] D. Singh, D. Sharma, S. L. Soni, S. Sharma, K. P. Sharma, A. Sharma & A. Jhalani, "A review on feedstocks, production processes, and yield for different generations of biodiesel," Fuel **262** (2020) 116553. https://doi.org/10.1016/j.fuel.2019.116553.

[11] T. Indika, B. Sandhya & S. Chanatip, "Biodiesel production in an autoclave reactor using waste palm oil and coconut coir husk derived catalyst," Renew. Energy **134** (2019) 125. https://doi.org/10.1016/j.renene.2018.11.030.

[12] K. Khan, N. Ul-Haq, W. U. Rahman, M. Ali, U. Rashid, A. Ul-Haq, F. Jamil, A. Ahmed, F. Ahmed, B. R. Moser & A. Ali, "Comprehensive comparison of hetero-homogeneous catalysts for fatty acid methyl ester production from non-edible *Jatropha curcas* oil," Catalysts **11** (2021) 1420. https://doi.org/10.3390/catal11121420.

[13] C. E. Akhabue & J. A. Ogogo, "Modelling and optimization of transesterification of palm kernel oil catalysed by calcium oxide derived from hen eggshell wastes," Ife J. Sci. **20** (2018) 127. https://doi.org/10.4314/ijs.v20i1.13.

[14] K. S. Nishant, S. Yashvir & S. Abhishek, "Optimization of biodiesel synthesis from Jojoba oil via supercritical methanol: A response surface methodology approach coupled with genetic algorithm," Biomass Bioenergy **156** (2022) 1. https://doi.org/10.1016/j.biombioe.2021.106332.

[15] B. O. S. Olive, B. E. Fabien, M. A. Edwige, N. P. M. & A. A. Ateba, "Physico-chemical and thermal characterisation of *Canarium schweinfurthii* Engl (Cs) shells," Int. J. Mater. Sci. Eng. **7** (2021) 9. https://doi.org/10.14445/23948884/IJMSE-V7I3P102.

[16] N. E. Cordelia, O. O. Dominic, N. U. Callistus & I. G. Austin, "Biodiesel synthesis from waste *Canarium schweinfurtii* oil (WCSO) catalyzed by thermal reinforced clay and its kinetics evaluation," Cleaner Mater. **6** (2022) 100145. https://doi.org/10.1016/j.clema.2022.100145.

[17] D. T. Adeyemi, A. Saleh, F. B. Akande, O. O. Oniya & F. A. Ola, "Determination of fuel properties of biodiesel from sand apple seed oil with automotive gas oil blend," J. Appl. Sci. Environ. Manage. **25** (2021) 1365. https://doi.org/10.4314/jasem.v25i8.12.

[18] S. J. M. Breig & K. J. K. Luti, "Response surface methodology: A review on its applications and challenges in microbial cultures," Mater. Today: Proc. **42** (2021) 2277. https://doi.org/10.1016/j.matpr.2020.12.316.

[19] K. M. Nameer, T. S. Ziad, A. J. Mohammed & K. S. Sami, "Effect of different extraction methods on physicochemical properties and antioxidant activity of virgin coconut oil," Mater. Today: Proc. **42** (2021) 2000. https://doi.org/10.1016/j.matpr.2020.12.248.

[20] B. H. Ketema, "Optimization of biodiesel production parameters from *Cucurbita maxima* waste oil using microwave assisted via Box–Behnken design approach," J. Chem. **2022** (2022) 8516163. https://doi.org/10.1155/2022/8516163.

[21] H. S. Muhammad, R. Agada, I. J. Ogaji & N. C. Ngwuluka, "Physicochemical characterization and fatty acids composition of four indigenous plant oils," Sci. Afr. **20** (2023) e01669. https://doi.org/10.1016/j.sciaf.2023.e01669.

[22] S. Sahu, K. Saikia, B. Gurunathan, A. Dhakshinamoorthy & S. L. Rokhum, "Green synthesis of CaO nanocatalyst using watermelon peels for biodiesel production," Mol. Catal. **547** (2023) 113342. https://doi.org/10.1016/j.mcat.2023.113342.

[23] D. Kalpana, J. H. Han, W. S. Park, S. M. Lee, R. Wahab & Y. S. Lee, "Green biosynthesis of silver nanoparticles using *Torreya nucifera* and their antibacterial activity," Arab. J. Chem. **12** (2019) 1722. https://doi.org/10.1016/j.arabjc.2014.08.016.

[24] K. Chanda, D. Cao, D. E. Fouad, A. H. Shah, A. Q. Dayo, K. Zhu, M. N. Lakhan, G. Mehdi & S. Dong, "Green synthesis, characterization and photocatalytic application of silver nanoparticles synthesized by various plant extracts," Arab. J. Chem. **13** (2020) 8248. https://doi.org/10.1016/j.arabjc.2020.01.009.

[25] A. K. Y. Aqeel, S. Achhaibar & S. Dinesh Kumar, "A hybrid RSM–GA–PSO approach on optimization of process intensification of linseed biodiesel synthesis using an ultrasonic reactor: Enhancing biodiesel properties and engine characteristics with ternary fuel blends," Energy **288** (2024) 129077. https://doi.org/10.1016/j.energy.2023.129077.

[26] A. N. Godswill, E. O. Prosper, A. I. Chinenye, F. Endrit, A. O. Jones, D. Y. Alfred & C. O. Pius, "RSM optimization and yield prediction for biodiesel produced from alkali-catalytic transesterification of pawpaw seed extract: Thermodynamics, kinetics, and multiple linear regression analysis," Digit. Chem. Eng. **6** (2023) 100066. https://doi.org/10.1016/j.dche.2022.100066.

[27] E. Kamran, H. Mashhadi, A. Mohammadi & B. Ghobadian, "Biodiesel production from *Elaeagnus angustifolia* L. seed as a novel waste feedstock using potassium hydroxide catalyst," Biocatal. Agric. Biotechnol. **25** (2020) 101578. https://doi.org/10.1016/j.bcab.2020.101578.

[28] C. Sanjurjo, P. Oulego, M. Bartolomé, E. Rodríguez, R. Gonzalez & B. A. Hernández, "Biodiesel from the microalgae *Nannochloropsis gaditana*: Optimization of the transesterification reaction and physicochemical characterization," Biomass Bioenergy **185** (2024) 107240. https://doi.org/10.1016/j.biombioe.2024.107240.

[29] A. Tanweer, D. Mohammed & K. B. Pradeep, "Optimization of process variables for biodiesel production by transesterification of flaxseed oil and produced biodiesel characterizations," Renew. Energy **139** (2019) 1272. https://doi.org/10.1016/j.renene.2019.03.036.

[30] J. Lestari, M. B. Rosana, F. E. Sondari, Y. H. Ju & S. Ismadji, "Production of biodiesel from sea mango (*Cerbera odollam*) seed using in situ subcritical methanol–water under a non-catalytic process," Int. J. Ind. Chem. **9** (2018) 53. https://doi.org/10.1007/s40090-018-0138-3.

[31] C. M. Stephen, F. M. Junior, I. Musa, C. A. Emilia & P. M. Kalu, "Assessment of proximate and physico-chemical potentials of crude kernel oil extracts of *Canarium schweinfurthii* Engl.," Niger. J. Pure Appl. Sci. **34** (2021) 3941. https://doi.org/10.48198/NJPAS/20.B13.

[32] F. Marcos, S. Carolina, E. V. Claudia, A. Felipe, V. Hugo & O. V. Jaime, "Avocado oil: characteristics, properties and applications," Molecules **24** (2019) 217. https://doi.org/10.3390/molecules24112172.

[33] B. R. Moser, D. Christina, B. B. Grigo, J. K. Winkler-Moser & M. D. Kenneth, "Production and evaluation of biodiesel from sweet orange (*Citrus sinensis*) lipids extracted from waste seeds from the commercial orange juicing process," Fuel **342** (2023) 127727. https://doi.org/10.1016/j.fuel.2023.127727.

[34] M. M. Ahmad, H. M. Kotb, S. Mushtaq, M. W.-U. Rehman, C. M. Maghanga & M. W. Alam, "Green synthesis of Mn + Cu bimetallic nanoparticles using *Vinca rosea* extract and their antioxidant, antibacterial, and catalytic activities," Crystals **12** (2022) 72. https://doi.org/10.3390/cryst12010072.

[35] D. A. Bopape, S. Mathobela, N. Matinise, D. E. Motaung & N. C. Hintsho-Mbita, "Green synthesis of CuO–TiO_2 nanoparticles for the degradation of organic pollutants: Physical, optical and electrochemical properties," Catalysts **13** (2023) 163. https://doi.org/10.3390/catal13010163.

[36] A. De & S. S. Boxi, "Application of Cu impregnated TiO_2 as a heterogeneous nanocatalyst for the production of biodiesel from palm oil," Fuel **265** (2020) 117019. https://doi.org/10.1016/j.fuel.2020.117019.

[37] M. F. Abdullahi, S. Y. Chin & Y. H. Taufiq-Yap, "CaO–TiO_2 mixed oxide catalysts for biodiesel production," Energy Convers. Manage. **101** (2015)

186. https://doi.org/10.1016/j.enconman.2015.05.027.

[38] Y. Wu, C. Xia, J. Cao, H. A. L. Garalleh, M. Garaleh, M. Khouj & A. Pugazhendhi, ‘‘A review on current scenario of nanocatalysts in biofuel production and potential of organic and inorganic nanoparticles in biohydrogen production,’’ Fuel **338** (2023) 127216. https://doi.org/10.1016/j.fuel.2022.127216.

[39] C. Sanjurjo, P. Oulego, M. Bartolomé, E. Rodríguez, R. González & B. A. Hernández, ‘‘Biodiesel production from the microalgae *Nannochloropsis gaditana*: Optimization of the transesterification reaction and physicochemical characterization,’’ Biomass Bioenergy **185** (2024) 107240. https://doi.org/10.1016/j.biombioe.2024.107240.

[40] N. O. Mascarenhas, M. A. Pereira, C. A. M. Pires, G. Simonelli & L. C. L. Santos, ‘‘Production, optimization, and evaluation of thermal stability of palm oil biodiesel produced using a natural coconut oil–based surfactant,’’ Biomass Convers. Biorefin. (2022). https://doi.org/10.1007/s13399-022-03102-y.

[41] S. Bharadwaj, A. V. L. Saia, S. Niju, M. Khadhar, M. S. B. & N. Anantharaman, ‘‘Optimization of continuous biodiesel production from rubber seed oil (RSO) using calcined eggshells as heterogeneous catalyst,’’ J. Environ. Chem. Eng. **8** (2020) 103603. https://doi.org/10.1016/j.jece.2019.103603.

[42] H. Balkis, R. Umer, H. Yun, T.-Y. Yun, L. I. Mohd & A. N. Imededdine, ‘‘Supermagnetic nano-bifunctional catalyst from rice husk: Synthesis, characterization and application for conversion of used cooking oil to biodiesel,’’ Catalysts **10** (2020) 225. https://doi.org/10.3390/catal10020225.